Journal of
MATERIALS RESEARCH

The mechanism of sputter-induced epitaxy modification in YBCO (001) films grown on MgO (001) substrates

Y. Huang, B. V. Vuchic, M. Carmody, P. M. Baldo, and K. L. Merkle
Materials Science Division, Argonne National Laboratory, Argonne, Illinois 60439

D. B. Buchholz, S. Mahajan, J. S. Lei, P. R. Markworth, R. P. H. Chang, and L. D. Marks
Department of Materials Science and Engineering, Northwestern University, Evanston, Illinois 60201

(Received 9 July 1997; accepted 25 January 1998)

The sputter-induced epitaxy change of in-plane orientation occurring in $YBa_2Cu_3O_{7-x}$ (001) thin films grown on MgO (001) substrates by pulsed organo-metallic beam epitaxy (POMBE) is investigated by a series of film growth and characterization experiments, including RBS and TEM. The factors influencing the orientation change are systematically studied. The experimental results suggest that the substrate surface morphology change caused by the ion sputtering and the Ar ion implantation in the substrate surface layer are not the major factors that affect the orientation change. Instead, the implantation of W ions, which come from the hot filament of the ion gun, and the initial Ba deposition layer in the YBCO film growth play the most important roles in controlling the epitaxy orientation change. Microstructure studies show that a $Ba_xMg_{1-x}O$ buffer layer is formed on top of the sputtered substrate surface due to Ba diffusion into the W implanted layer. It is believed that the formation of this buffer layer relieves the large lattice mismatch and changes the YBCO film from the 45° oriented growth to the 0° oriented growth.

I. INTRODUCTION

Grain boundary junctions in high-T_c superconductor materials have attracted much attention in recent years. Many methods have been developed to fabricate grain boundary junctions (GBJ's). Among others, the step edge method,[1,2] bicrystal method,[3–5] and biepitaxy method[6,7] have been extensively studied. Junctions made by the bicrystal method are presently being used in commercial devices. The disadvantage of these fabrication processes is that they are all quite complex and/or expensive. Therefore there is a need for simpler and inexpensive procedures. The method to be discussed in this paper is similar to but much simpler than the biepitaxy technique. This method uses low-energy ion sputtering to selectively treat the substrates. Under specific synthesis conditions the superconductor films grow with different in-plane orientations on the sputtered and nonsputtered substrate areas and thus form GBJ's between the two areas. The change of epitaxy orientation by ion sputtering will be termed "sputter-induced epitaxy modification" (SIEM) and the method to form GBJ's by this change, the SIEM method.

The SIEM phenomenon was first observed by Chew *et al.*[8] They grew *c*-axis normal $YBa_2Cu_3O_{7-x}$ (YBCO) films on MgO (001) substrates by the coevaporation method. On nonsputtered substrates they observed the in-plane orientation relation to be $[100]_{YBCO}//[100]_{MgO}$, but on substrate sputtered by low energy Ar ions at ~200 °C, the orientation relation became $[110]_{YBCO}//[100]_{MgO}$. Thus, the YBCO film assumed a 45° rotation of in-plane rotation on sputtered substrates. It should be noted that Chew *et al.* were not able to reproduce their results after making variations to their processing chamber.[9] Vuchic *et al.*[10] observed the same type of orientation change in the YBCO films grown on MgO (001) by pulsed organo-metallic beam epitaxy (POMBE). Using the sputter-induced epitaxial rotation Vuchic *et al.* fabricated 45° GBJ's and systematically investigated the microstructure and electrical properties of the junctions.[11,12]

To be concise, hereafter we refer to the in-plane orientation relations by the angle between the YBCO [100] and MgO [100]. Hence, in this notation the orientation relation $[100]_{YBCO}//[100]_{MgO}$ (sometimes called cube-on-cube) is a "0° orientation" and $[110]_{YBCO}//[100]_{MgO}$ is a "45° orientation."

Relative to these early observations, Buchholz *et al.* recently reported different YBCO/MgO orientation relations in films grown by the POMBE method: Under standard synthesis conditions the YBCO films on the nonsputtered MgO regions are 45° oriented and those on the sputtered regions are 0° oriented.[13] The result is verified by several experimental methods and can be routinely reproduced. It is believed that the difference from previous results was caused by some unknown changes in the processing chamber and by paying particular attention to the deposition of the initial atomic layers. It is evident that the factors that affect the YBCO growth orientation on MgO (100) are quite complex and the task for controlling the orientation by ion sputtering is not simple. In order to understand the factors involved

and reproducibly control the growth orientation it is essential to know the mechanism of the sputter-induced epitaxy modification. This is important not only for further improvement of the GBJ quality, but also for extension of the SIEM method to other systems of different film/substrate combinations and/or synthesis routes.

Before we discuss the mechanism of SIEM, a brief review of the previous studies on YBCO growth on MgO is helpful. Many efforts have been made to grow YBCO films on MgO (001) substrates and to study the orientation relation, film/substrate interfaces, and YBCO grain boundaries.[14–34] A variety of film growth methods, different growth conditions (substrate temperature, oxygen partial pressure, growth rate, etc.), and substrate treatments (polishing, acid-etching, annealing, ion-sputtering, etc.) have been used. In most cases *c*-axis oriented films were obtained because *c*-axis films are thermodynamically more favorable and the growth rate is much higher in a-b direction than in c-direction. Many of the early films were polycrystalline and contained grains with their a-b axes rotated from the substrate [100] direction by several preferred angles. Among those angles, 0° and 45° are most frequently observed. The initial stage of the film growth has been studied by several authors.[26,29,31,35] The growth mode was identified as true 3-D island growth.[26,29] The YBCO/MgO interface under the 0° and 45° oriented grains and the 45° tilt boundary between these two kinds of grains were extensively studied.[12,22,28] In recent years, single-crystal-like YBCO films on MgO (001) substrates with their a-b axes locked in two perpendicular directions were obtained. It was reported that the films with in-plane orientation of 0°[14] or 45°[33] were obtained by pulsed laser ablation and magnetron sputtering, respectively. Some authors were able to obtain both 0° and 45° oriented films under different substrate treatments and growth conditions by pulsed laser ablation[20] and coevaporation.[8] By using the POMBE method, combined with the selective ion-sputtering treatment of the substrate surface, the present authors were able to obtain 0° and 45° oriented YBCO films at pre-selected substrate regions simultaneously.[13,36]

The structure of YBCO/MgO interfaces is often studied to provide insight into the reasons for the different orientation relations. Near coincident site lattice (NCSL) theory has been used to model the interface.[17,28,32] and to rationalize the observed orientation angles. In these studies the lattice misfits for those observed angles were calculated. It is found that in 0° orientation the lattice misfit between YBCO and MgO is quite large (8.2–10.2%). This may lead to a high strain energy at the interface. The existence of ⟨100⟩ steps on the MgO surface has been proposed as a reason why the large misfit 0° orientation is still present.[24,28] At all the observed angles other than 0° the lattice misfits are smaller than 3%. For example, at the 45° orientation a lattice misfit of 2.9% is obtained by matching four MgO (200) lattice planes with three YBCO (110) planes. To accommodate the different number of the matched planes, interface dislocations should be formed between the YBCO and MgO lattices. The small lattice mismatch and formation of the interface dislocations that relieve strain should result in a smaller strain energy at the 45° oriented interface than at the 0° interface. These interface dislocations have been observed in polycrystal films[17,27] and single-crystal-like films obtained with the SIEM method.[16,37] In brief, previous workers made considerable efforts to obtain single crystal YBCO films and control their orientation on MgO, but no systematic investigations have been carried out to study the mechanism of the orientation control.

Regarding the ion-sputter-induced orientation change, many processes occur during the low-energy ion bombardment of the surface. Among them the most important effects are surface topology change, ion implantation and modification of surface structure, and chemistry. These effects have been discussed by Vuchic *et al.*[12] and Buchholz *et al.*[36] and will be further investigated in this work with detailed analysis of new experimental results. The effects of the different sputtering conditions are explored by a series of film growth experiments.

II. EXPERIMENTAL

The substrates used in this work are polished MgO (100) chips of epitaxial quality obtained from Coating and Crystal, Inc. The ion source for the sputter treatment is a low-voltage (50–1200 V) 3 cm diameter Kaufman-type ion gun with graphite accelerating grids and a tungsten filament, made by IonTech, Inc. The base vacuum of the sputtering chamber is better than 1×10^{-6} Torr. During ion sputtering, an Ar flow of 2.5 sccm is fed into the gun and the vacuum in the chamber is about 2×10^{-4} Torr. A typical ion sputtering condition is 500 eV ion beam at 90° incidence for 4 min with a beam current density of about 1 mA/cm^2. Different ion energies, incident angles, and milling times are also used to study the effect of these parameters on the resulting film epitaxy. An ion gun which employs an rf field to ionize the Ar gas, as opposed to the hot tungsten filament, is also used to isolate the effect of the tungsten filament.

To fabricate 45° tilt grain boundaries, the substrate is patterned with a standard photolithography procedure to define the regions to be sputtered. YBCO films are then grown on the substrates. The 45° tilt grain boundaries are formed between the sputtered and nonsputtered regions.

The details of the POMBE method and the setup for the YBCO thin film growth have been reported elsewhere.[38] Briefly, the precursors are pulsed onto the substrates via a set of computer controlled valves. The

pulse sequence and length are programmed into the computer. This allows very fine control over the type and amount of the precursors delivered to the substrate. The organo-metallic source materials used are $Y(dmp)_3$, $Ba(hfa)_2(tet)$, and $Cu(dpm)_2$ for the deposition of Y, Ba, and Cu, respectively. Usually, the precursors are pulsed in the sequence of $Ba-(Cu-Y-Cu-Ba-Cu-Ba-)_n$, where n is the number of times the sequence in the parentheses is repeated. The reason for the initial Ba pulse is to form a "seed layer" on the sputtered region. Only when the initial amount of Ba is kept within a certain range can one create the desired orientation relations and form 45° boundaries. The details concerning the effect of this first Ba layer have been reported elsewhere[13,36] and will be discussed further in the next section. During film growth the substrates are heated to a temperature of 670 °C to 685 °C. The deposition ambient is a water-doped oxygen plasma that can be controlled by adjusting microwave power and oxygen partial pressure.

The in-plane film orientation is determined by several methods, including four-circle x-ray diffractometer (ϕ scan), electron backscattering patterns (EBSP), and selected area diffraction (SAD) in TEM, depending on the size of the areas to be examined.

RBS is used to analyze the surface composition of the sputtered substrates and the initial stage of film growth. The RBS experiments are done at the 2 MeV Tandem National Electrostatics ion accelerator facility at Argonne National Laboratory. The energy of the He ion beam used in the experiments is 1.6 MeV. The angle between the beam axis and the sample normal is 10°. An Au–Si surface barrier detector with an energy resolution of 16.5 keV (FWHM) is used to detect the backscattered ions. The detector is positioned at 135° with respect to the beam axis. To simulate a RBS spectrum the spatial distribution of the elements in the surface layer of the sample should be taken into account. In the experiments concerning the initial stage of film growth, the deposited layer is assumed to be directly at the sample surface. In the case of sputtering, a spatial distribution calculated from the TRIM program is used. The concentrations of the elements are then determined by an interactive procedure fitting the simulated RBS spectra to the experimental spectra.

The surface morphology of the sputtered and nonsputtered substrates is examined by atomic force microscopy (AFM) and high resolution TEM (HREM). The AFM instrument used in this work is a Nanoscope III, made by Digital Instruments, Inc. The resolution of the AFM is about 10 nm. For details smaller than 10 nm, HREM cross-section images are taken.

Conventional and high resolution TEM are employed to examine the composition and microstructure of the YBCO/MgO interfaces and the boundary between the 0° and 45° oriented areas. The sample preparation procedures has been reported elsewhere.[39] Briefly, an array of alternate sputtered and nonsputtered rectangular regions, 10 μm wide, are created on the MgO substrate. The long edge of the rectangular regions is along one of the MgO ⟨100⟩ directions. When YBCO films are grown on this substrate an array of boundaries along the MgO ⟨100⟩ direction with 10 μm spacing are formed. This pattern geometry guarantees that many boundaries will be present for observation in the completed TEM sample. The junction array is then cross-sectioned, mechanically polished to foils about 10 μm thick, and ion milled to electron transparency. To minimize the damage caused by possible elevated temperature the samples are cooled to liquid-nitrogen temperature during the ion milling. Since many boundaries are formed in the sample and the whole width of the cross section is thinned to electron transparency, many boundaries can be observed in a single sample.

The high resolution microscopy in this work is done on a JEOL-4000EXII and a Hitachi H-9000. A Philips CM-30 and a Hitachi HF-2000 are used for microanalysis. The latter has a field emission electron gun, a Link system EDX analyzer, and an EMiSCAN system that allows easy acquisition of the elemental line profile data. When acquiring the line profile, a beam size of 2 nm is used, giving a spatial resolution of the microanalysis better than 2 nm. Typically, a spectrum profile is obtained in the acquisition and the elemental profiles are obtained by processing the data after the acquisition.

III. RESULTS AND DISCUSSION

Under favorable growth conditions good single-crystal-like YBCO thin films with their c-axis aligned with the substrate surface normal (MgO[001]) and their a-, b-axis locked in two perpendicular directions can be readily obtained. The in-plane orientation of the films, with respect to the substrate, are different in the nonsputtered and sputtered regions. As shown by ϕ-scan x-ray diffraction, the in-plane orientations of the films are $[110]_{YBCO} // [100]_{MgO}$ (45° orientation) for the nonsputtered substrate and $[100]_{YBCO} // [100]_{MgO}$ (0° orientation) for the sputtered substrate. In some unfavorable conditions mixed orientations occur. In those situations the fraction of area for each orientation over the total surface can be determined from the x-ray diffraction data. The accuracy of the x-ray data allows detection of minor orientation occupying less than 1% of the total surface area.

A. Effect of surface morphology change

The effects of the three most important sputtering parameters on the occurrence of SIEM are explored by film growth experiments. Ion beam energy, ion incident

angle, and sputtering time are varied, followed by examination of the YBCO films grown on the sputtered MgO substrates. In the incident-angle experiment the sample is put at a random azimuth during sputtering to avoid possible channeling effects. The results of the experiments are compiled in Table I. The "Yes" in the fourth column of the table means that YBCO films are grown in 0° orientation on at least 97% of the sputtered substrate surface.

It is easy to see from Table I that SIEM does not occur under the following conditions: when the ion energy is smaller than 100 eV; when the incident angle is smaller than 60°; or when the sputtering time is equal to or shorter than 2 min. The thresholds in ion energy and sputtering time are easy to understand: when the ion energy is very low and/or the sputtering time is very short, the effect of the ion beam on the substrate is too small to give rise to any major change on the substrate surface and hence SIEM does not occur. The reason for a threshold in the ion beam incident angle, however, is not as straightforward. It is well known that ion sputtering removes materials much faster at incident angles of 20–40° than at perpendicular incidence. In other words, there should be a larger surface change at those shallower incident angles than at 90° incidence. Therefore, the fact that SIEM does not occur at incident angles less than 45° seems to imply that the surface morphology change is not a major factor that causes SIEM: if surface morphology changes, such as formation of steps, ledges, and facets, were controlling the SIEM mechanism, SIEM would occur more easily on the surface sputtered at intermediate angles. The greater removal of the surface layer at low angle ion sputtering will, however, also effect ion implantation into the substrate surface. This effect will be discussed in greater depth in Sec. III. B.

TABLE I. Occurrence of sputter-induced epitaxy modification in YBCO films on MgO (001) substrate at different sputtering conditions.

Ion energy (eV)	Incident angle	Time (min)	SIEM (yes/no)
50			N
100			Y
200			Y
300	90°	3	Y
400			Y
500			Y
600			Y
	10		N
	30		N
500	45	4	N
	60		Y
	75		Y
	90		Y
		1	N
		2	N
		3	Y
300	90	4	Y
		5	Y
		6	Y
		9	Y

The actual surface morphology changes caused by ion sputtering were examined by AFM and cross-section TEM. The AFM results are shown in Fig. 1. The image in Fig. 1(a) shows the surface of the as-polished MgO, which is very flat with the height fluctuation on the surface smaller than 1 nm. After ion sputtering the substrate becomes much rougher with height fluctuation as large as 5–10 nm [Fig. 1(b)]. This difference between nonsputtered and sputtered surfaces, however, is largely diminished by a 30 min annealing in an oxygen plasma at ~670 °C that is routinely performed before YBCO film growth. After the annealing both nonsputtered and sputtered substrates have similar surface morphology of relatively larger bumps 0.1–0.3 μm in size [Figs. 1(c) and 1(d)]. The only difference is the bump height. The average bump height is about 6 nm on the nonsputtered substrates and about twice this value on the sputtered substrates.

Since the lateral resolution of AFM is relatively poor, the cross-sectional TEM is used to examine the finer detail in the surface morphology change. No significant difference regarding atomic-scale features can be seen between these two substrates, except that the long-range (>100 nm) height fluctuation is larger on the sputtered surfaces than on the nonsputtered surfaces. Since the initial growth of the YBCO films is an atomic-scale process, the surface morphology features which affect the film orientation must be on the atomic scale. Therefore, the fact that TEM observation shows no significant difference in the atomic-scale surface morphology reinforces the conclusion reached above that the surface morphology change caused by ion sputtering is not an important factor in SIEM.

B. The surface composition change induced by ion sputtering

The composition change of the substrate surface layer during ion sputtering was examined by RBS. Figure 2(a) shows a typical RBS spectrum of the MgO substrate sputtered with an ion gun that employs a hot W filament to ionize the Ar ion. In addition to the high Mg and O edges, there are two small extra peaks in the spectrum that correspond to Ar and W. It is believed that the Ar and W are introduced into the substrate by the ion irradiation since RBS of the nonsputtered MgO does not show these two elements; see Fig. 2(b). The source of the W must be the hot W filament of the ion gun. When the ion gun is on, electrons are emitted by the hot filament, accelerated by the "discharge" electric field and forced to move in spiral orbits by a magnetic field. Ar atoms in the discharge chamber are ionized by these electrons. At the same time some W atoms are evaporated or sputtered

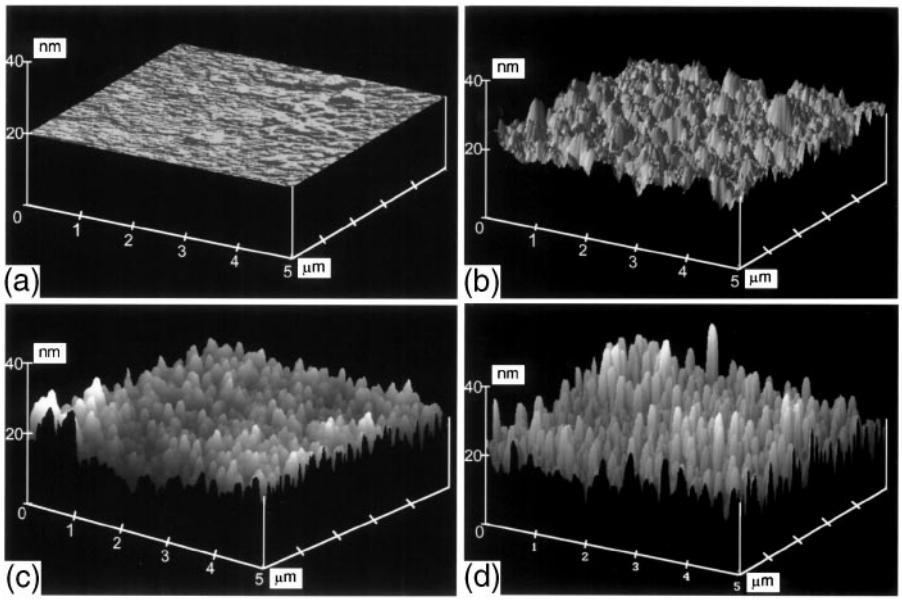

FIG. 1. AFM images of (a) the as-polished MgO surface before annealing; (b) the sputtered MgO surface before annealing; (c) the polished MgO surface after annealing; (d) the sputtered MgO surface after annealing.

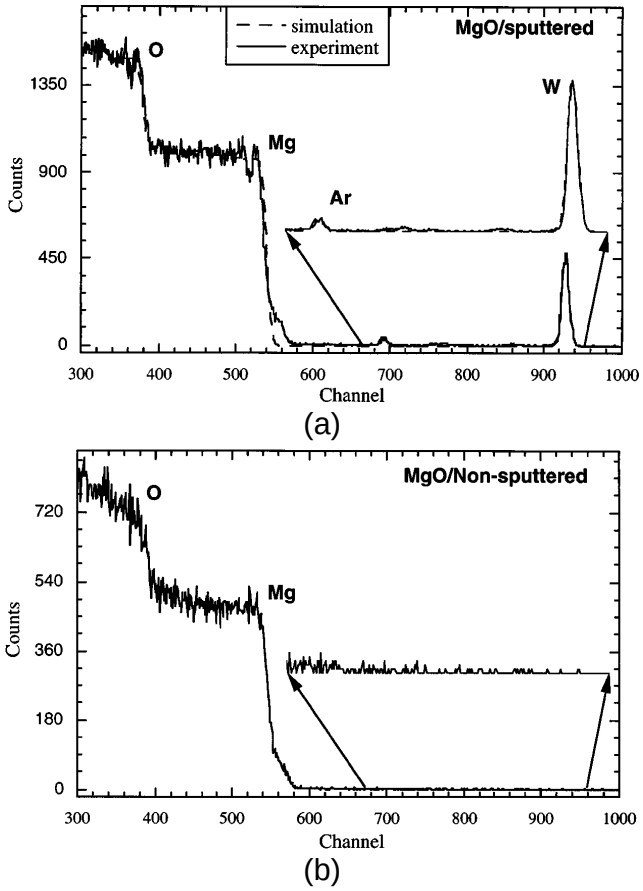

FIG. 2. (a) The solid curve is an RBS spectrum of a sputtered MgO surface, showing small Ar and W peaks. The broken curve is the simulation of the spectrum corresponding to 1.1 monolayer of Ar and 0.77 monolayer of W; (b) RBS spectrum of a nonsputtered MgO surface showing no Ar and W peaks.

from the hot filament and may also be ionized. These W ions are accelerated by the gun acceleration field along with the Ar ion beam and bombard the substrate. We did observe considerable consumption of the W filament during sputtering. When the ion beam emission current is kept constant, the filament-heating current continuously decreases at a rate of about 1% per 10 min, indicating that the filament is getting thinner at a fairly fast rate and thus a considerable amount of W may be introduced into the Ar ion beam.

Before calculating the concentrations of W and Ar in the MgO surface layer from the RBS spectra, their spatial distribution is modeled by a TRIM code Monte Carlo simulation. The results show that the Ar and W ions are implanted into the substrate and the peak concentrations are at depths of ~1 and ~2 nm, respectively. However, under typical sputtering conditions the ion beam is perpendicular to the substrate surface and parallel to its [001] direction. Hence, strong ion channeling is expected to occur and the actual distribution of W and Ar may be considerably deeper than the first order TRIM values. In addition, since the substrate materials are continuously milled away by the ion beam during implanting, the distribution peaks are smeared out. Therefore, the final distribution of the Ar and W is assumed nearly uniform over the top 3–4 nm layer of the substrate. This uniform distribution is used for the RBS spectrum simulation. The concentrations of Ar and W in this layer are determined by matching a simulated RBS spectrum with the experimental RBS spectrum. Under typical sputtering condition (500 eV ion beam at 90° incidence for 4 min), the total amounts of Ar and W in the surface layer are

approximately 1.1 and 0.77 monolayers, respectively. Considering the Ar ion beam current of 1 mA/cm^2, less than 0.2% of the Ar ions stay in the substrate after sputtering. The emission rate of W is not known, but it must be much smaller than for Ar. Since the final W concentration is close to the Ar concentration, the implantation ratio of W ions must be much higher than that of Ar ions. This phenomenon can be attributed to several effects, including the larger implantation depth of the W ions and the smaller mobility of W ions in the substrate surface layer due to their larger mass and stronger interaction with substrate atoms.

The difference between the mobility of Ar and W ions in the substrate surface layer can also be seen from the change of their concentration with sputtering time. Both Ar and W concentration in the surface layer increase with sputtering time, but the Ar concentration saturates in less than 1 min while the W concentration continues to increase up to 10 min of the sputtering time [Fig. 3(a)]. The early saturation of Ar ions can be understood by considering the milling effect of the subsequent Ar ion beam. During the sputtering process

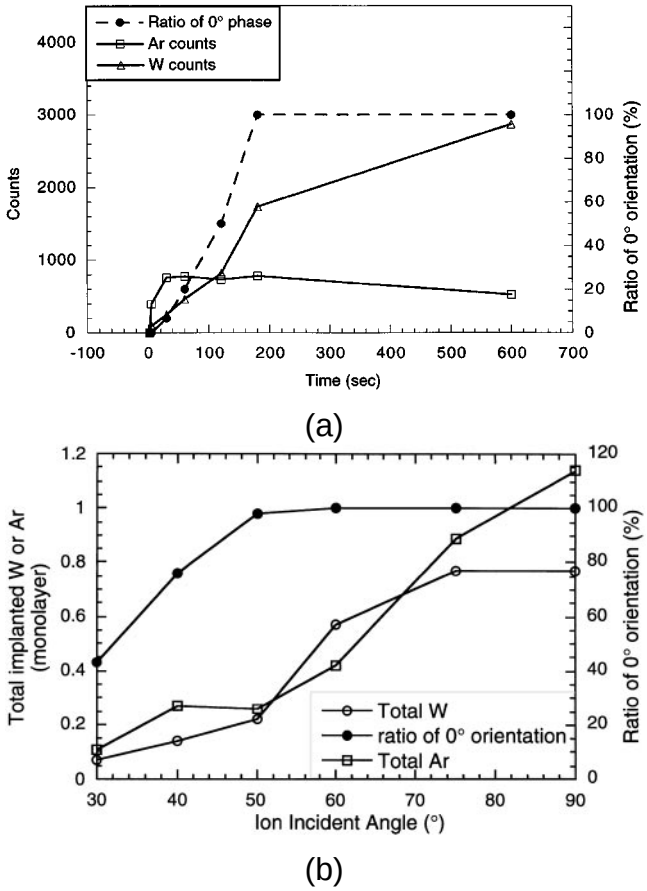

FIG. 3. (a) Variation of Ar and W concentration with sputtering time as determined by RBS. The Ar concentration saturates in less than 30 s of sputtering. (b) Ar and W concentration both increase with ion incident angle. The ratio of the 0° oriented phase on the sputtered surface shows the same trend as the W concentration.

previously implanted ions are partly removed from the substrate while new ions are implanted in the substrate. After an initial transition period a steady-state concentration will be reached. The higher the removal rate of the implanted ions, the faster the final concentration is reached. The Ar ions are more loosely bound and implanted to a shallower depth than the W ions, therefore the probability for the Ar ions being removed from the MgO surface layer by the subsequent ion sputtering is much greater than that for the W ions. In addition, since Ar is an inert gas, it may be stable in the surface region only in the form of subsurface clusters from which Ar may eventually escape from the substrate into the vacuum. Both effects cause higher removal rates of Ar by the sputtering; therefore the steady-state concentration of Ar is reached much faster than that of W.

The early saturation of Ar concentration suggests that Ar implantation may not be important to the occurrence of SIEM. No SIEM occurs for a 1 min exposure to the ion beam (see Table I), and the Ar concentration has already become saturated at this stage [see Fig. 3(a)]. The W concentration, on the other hand, does not saturate until after SIEM is observed and therefore may have an important effect on the change of the YBCO orientation. Shown in Fig. 3(b) are the W concentration and the fraction of the 0° oriented phase; both increase with increasing ion incident angle. This again suggests a connection between W implantation and the occurrence of SIEM. To further explore this connection, YBCO films were grown on MgO substrates sputtered by an Ar ion gun that uses an rf field to generate the Ar ions; hence no W ions are generated or implanted into the substrates. All other conditions were the same as with the tungsten filament ion gun. In the resultant films the fraction of the 0° phase is greatly diminished from that observed when substrates are sputtered with a tungsten filament ion gun and only slightly larger than that of the nonsputtered case, indicating that W-free Ar ion sputtering has little effect on the occurrence of SIEM (see Fig. 4). Thus, W implantation appears essential to SIEM.

In the POMBE procedure the substrate is always treated with an oxygen plasma at ~670 °C for 30 min before the growth of YBCO film. To determine if the implanted ions are lost in this treatment, sputtered substrates were examined by RBS both before and after the predeposition treatment. The result indicates that most of the Ar and W remain in the substrate after the plasma treatment and are not sputtered away by the oxygen plasma.

C. Effects of the initial film growth conditions

The YBCO film growth conditions affect the YBCO film orientation on MgO. The POMBE deposition system delivers the metal precursors to the substrate in a serial

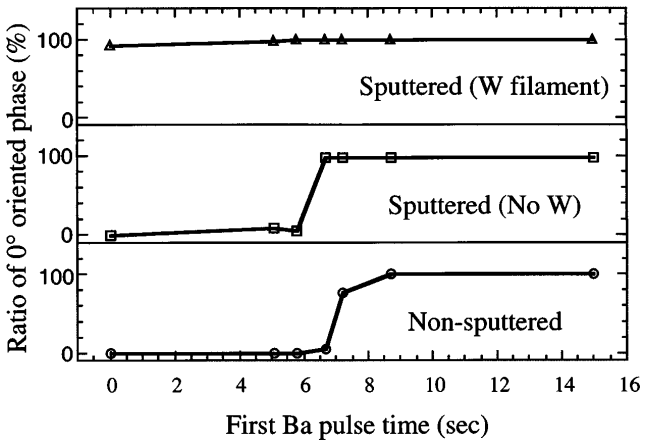

FIG. 4. The ratio of 0° oriented YBCO films on the substrate surface changes with the length of the initial Ba pulse in the POMBE growth. The three curves show the change under three different substrate treatment conditions.

sequence of discrete pulses. The type and amount of metal precursor in each pulse can be controlled. An important factor in the control of film orientation is the type and amount of precursor in the initial film layer. To obtain SIEM, a Ba layer of a certain thickness needs to be deposited first. In the POMBE system this is realized by controlling the length of the first Ba precursor pulse under a calibrated constant flow rate. The dependence of the film orientation on the first Ba pulse length is illustrated in Fig. 4, which plots the ratio of 0° oriented areas over the total substrate surface versus the first Ba pulse time. When this ratio is 0, the whole film is oriented at 45°. The three curves in the figure correspond to the MgO (001) substrates nonsputtered, sputtered by a W-free Ar ion gun, and sputtered by an Ar ion gun with a W filament, respectively. The incorporation rate of Ba atoms into the deposited film is about 0.13×10^{15} Ba/cm^2 s.

For all three types of substrates the YBCO films grow entirely in 0° orientation when the initial Ba pulse is longer than 9 s. This means that if we deposit a sufficient amount of Ba onto the MgO surface before the YBCO growth, we always get 0° oriented YBCO films regardless of substrate treatment. This phenomenon can be called "Ba-induced 0° growth."[36] When the initial Ba pulse is short, however, the film orientation can be different. For the two W-free surfaces there is a critical Ba pulse length below which the resultant YBCO film switches to 45° orientation. The switching of the orientation is quite abrupt. On the nonsputtered substrate, for example, the YBCO film changes from 100% of 0° orientation to 100% of 45° orientation when the initial Ba pulse decreases from 8.6 to 5.7 s. This gives the critical Ba pulse length for a nonsputtered substrate as about 5.7 s, which corresponds to a critical Ba coverage of 0.74×10^{15} Ba/cm^2 or 1.1 monolayers of BaO. For the substrate sputtered by an ion gun with a W filament the films are always grown in 0° orientation. Even when the deposition was started with a Y layer (i.e., a Ba pulse time of 0 s), more than 99% of the films grows with 0° orientation. In this case we can say that the critical Ba pulse length is zero. The change of the critical Ba pulse length by the sputtering forms a time window from 1 s to 5.7 s. Within this window one can grow the 0° oriented phase on regions sputtered with a W filament ion gun and the 45° oriented phase on the nonsputtered regions simultaneously. This makes the fabrication of the 45° tilt boundary with the SIEM method possible.

The phenomenon of "Ba-induced 0° growth" has been explained in terms of the initial growth behavior of BaO on the MgO (001) surface.[36] In a study of BaO growth on MgO (001), Cotter *et al.*[35] found that for Ba coverage less than a critical value (2–3 monolayers), the Ba atoms are substitutionally incorporated into the MgO lattice and the surface structure of the substrate remains unchanged. For Ba coverage greater than the critical value, an epitaxial BaO overlayer was formed. The *c*-axis of this overlayer is aligned with that of MgO and the in-plane orientation relation is $[110]_{BaO}//[100]_{MgO}$. The above observation was justified by a calculation of the heat of segregation.[40] Their calculations show that the formation of a BaO overlayer is energetically favorable over substitutional incorporation as the Ba coverage exceeded a critical coverage. Using Cotter's results, Buccholz *et al.*[13,36] proposed a model for the Ba-induced 0° growth. They believed that Cotter's critical Ba coverage for BaO overlayer to form corresponds to the critical initial Ba pulse length in the POMBE growth. Below this critical Ba coverage the surface retains the MgO (001) structure and the YBCO films are grown in the 45° orientation. When more Ba is deposited onto the surface, the concentration of the substitutional Ba atoms in the substrate surface layer will finally reach a saturation point and a BaO overlayer starts to form over the Ba saturated MgO layer. The subsequent YBCO films grow on the BaO overlayer with the orientation relation $[100]_{YBCO}//[110]_{BaO}$, giving the overall 0° orientation relation between YBCO films and the MgO substrate.

To explore the above model, TEM is used to examine a 0° oriented YBCO/MgO interface formed on a nonsputtered MgO substrate by depositing an extra amount of Ba in the initial stage of film growth. Figure 5 is a cross-section HREM image of this interface. This image shows that the top layer of the substrate has the same lattice fringes as the bulk MgO, except for some modification in contrast. It appears that this layer corresponds to the Ba saturated MgO top layer. Above this layer we expect to see a BaO overlayer. However, we did not see this overlayer in the image, even if the length of the first Ba pulse was as long as 30 s, corresponding

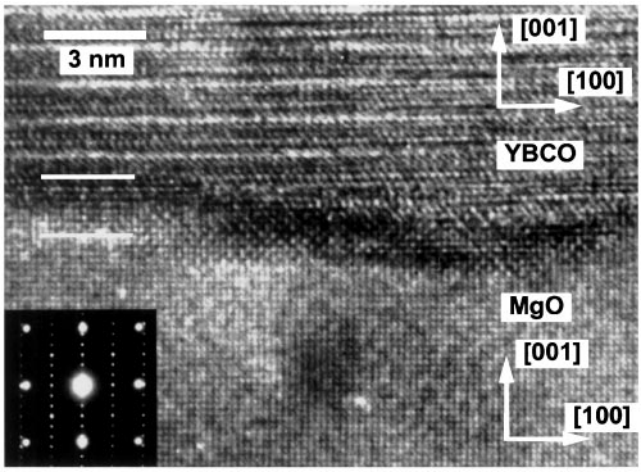

FIG. 5. Cross-sectional HREM image of the 0° oriented YBCO/MgO interface induced by extra amount of Ba deposition in the initial stage of the film growth.

to more than 6 monolayers of BaO. The elemental line profile across the interface obtained by high resolution EDX also shows no extra Ba-rich layer at the interface. A possible explanation for the absence of the BaO layer is that it disappears in the subsequent film growth process. Since Ba is one of the constituents of YBCO, diffusion may occur under the high temperature during the synthesis so that the extra Ba is incorporated into the YBCO film. The initial existence of this BaO layer, however, must cause the 0° orientation in the YBCO film.

Since extra initial Ba deposition leads to 0° growth, one could propose that the ion sputtering might increase Ba production on the sputtered areas and cause a "Ba-induced 0° growth". A possible mechanism is that an enhanced Ba deposition could result from an increase in the adsorption and/or decomposition rate of the Ba precursor by sputter-induced defects, such as steps and ledges that could increase the reaction rate, or by creating a surface chemical environment which is more favorable for the decomposition. If this speculation were correct, the mechanism of SIEM would be a form of "Ba-induced 0° growth".

In order to find out whether or not this is indeed the case, a critical experiment was performed. In this experiment only the initial Ba layer was simultaneously deposited onto sputtered and nonsputtered substrates, and the resultant Ba concentrations on these two substrates were measured by RBS. No significant difference between the two substrates was found. This indicates that ion sputtering does not increase Ba deposition on the substrate surface. Therefore, the mechanism of SIEM is not a form of "Ba-induced 0° growth".

D. Microstructure of the YBCO/MgO interfaces

A possible mechanism of SIEM is that the Ar ion sputtering and W implantation may cause some kind of structural changes in the surface MgO lattice and/or form a buffer layer at the surface that relieves the large lattice mismatch associated with the 0° growth. In order to characterize these structural changes, HREM is used to examine the 45° tilt grain boundaries fabricated with the SIEM method and the YBCO/MgO interfaces in the nonsputtered and sputtered regions.

HREM imaging shows a remarkable change in the interface structure after ion sputtering. Figure 6 is a cross-sectional TEM image of the root part (near the film/substrate interface) of a 45° tilt grain boundary formed between the sputtered and nonsputtered regions. The detailed structure of this boundary has been discussed elsewhere.[16] What we want to show here is the difference in the YBCO/MgO interfaces on the two sides of the boundary. In the nonsputtered region the interface is sharp, but in the sputtered region a layer of different contrast is formed at the interface. Figures 7(a) and 7(b) represent closer views of these two types of interfaces. The interface in the nonsputtered samples [Fig. 7(a)] is sharp and clean. The YBCO films grow directly on the MgO surface. There are no reaction products or intermediate layer at the interface. Although Ba is deposited as the initial layer of the YBCO growth, no extra layer is observed at this interface. It is believed that the initial Ba layer is incorporated into the YBCO layers in the subsequent growth process. The periodical features at the interface indicated by arrows suggest the formation of interfacial dislocations that match every four MgO [200] planes with three YBCO [110] planes. The interface in the sputtered samples [Fig. 7(b)], on the other hand, is not sharp. It is characterized by an intermediate layer 3–6 nm thick. This layer displays different lattice fringes compared to other parts of the sample, indicating that it has a structure different from either YBCO or MgO.

In addition to the difference in lattice structure, the elemental composition and spatial distribution near

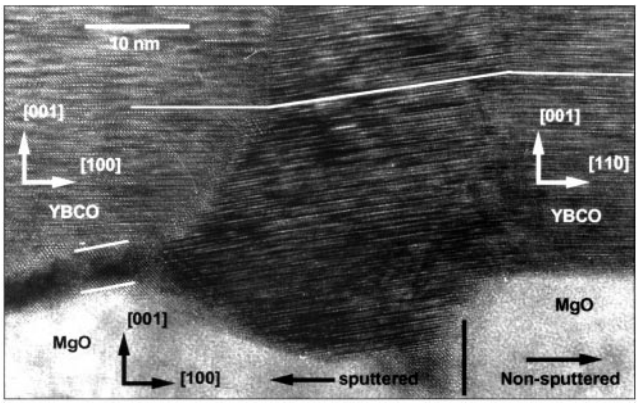

FIG. 6. HREM image of the root part of a 45° grain boundary formed by the SIEM method. Notice that the YBCO/MgO interfaces in the two sides of the boundary are different.

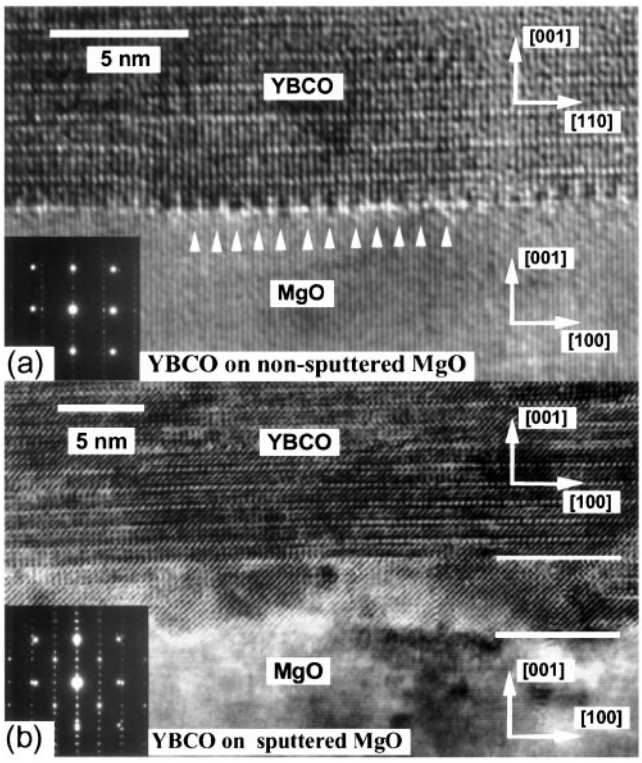

FIG. 7. YBCO/MgO interfaces in (a) nonsputtered MgO region and (b) sputtered MgO region. Note that the periodical contrast features indicated by arrows in (a) are formed by interface dislocations and that there is an intermediate layer formed between YBCO and MgO in (b).

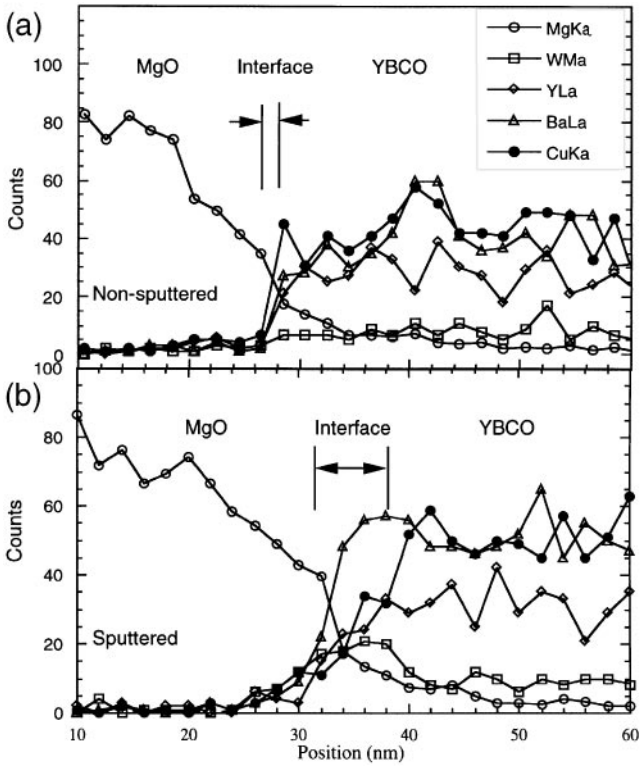

FIG. 8. Elemental line profile by high resolution EDX across the YBCO/MgO interfaces in (a) nonsputtered region and (b) sputtered region.

the interface regions are also different in the nonsputtered and sputtered samples. This can be seen from the elemental line profiles shown in Fig. 8, which are obtained by high spatial resolution EDX line scan. At both interfaces the Mg concentration drops down slowly as the probe is moved from the MgO side to the YBCO side, indicating some degree of Mg diffusion into YBCO. The concentration profile of Y, Ba, and Cu, however, is different between the nonsputtered and the sputtered interfaces. In the nonsputtered sample the concentrations of the three elements change abruptly as the probe crosses the interface, indicating a sharp YBCO edge. In other words, there is no diffusion of Y, Cu, or Ba into the MgO. In the sputtered sample, however, the Ba concentration increases a few nanometers ahead of Y and Cu concentration while the probe is moved from MgO to YBCO, indicating a Ba-rich layer a few nm thick at the interface. It is believed that this Ba-rich layer corresponds to the intermediate layer observed in the HREM images. The major composition of this layer is a mixture of barium, magnesium, and oxygen, with relatively small amount of yttrium and copper. The molecular formula of this layer could be written as $Ba_xMg_{1-x}O$. It is evident that the formation of this layer is caused by Ba diffusion from the deposited layer into the substrate. The first layer Ba deposition will definitely help in the formation of this intermediate layer. This is consistent with the fact that some length of the first Ba pulse in the POMBE growth is essential for the orientation change to occur. Also observed in the narrow (a few nm wide) YBCO/MgO interface region of the sputtered sample is a small amount of W. No W is observed at the nonsputtered interface. This fact is consistent with the RBS result mentioned in Sec. III. B and suggests the critical effect of W in the formation of the Ba-rich intermediate layer.

E. The mechanism of sputter-induced epitaxy modification

In the above sections we have found that the W ion implantation associated with the ion sputtering and the first Ba layer in the YBCO film growth are the two most important factors for the occurrence of SIEM. We also observed a large difference in the atomic-scale structure of the YBCO/MgO interface between sputtered and nonsputtered regions. In the sputtered region a Ba-rich intermediate layer is observed, which has the same thickness as the W implanted layer. From these experimental results, the process occurring on the MgO surfaces in the early stage of YBCO growth and the mechanism by which the different growth orientations on the sputtered and nonsputtered substrates are obtained can be described as below. On the nonsputtered MgO the

small amount of the initial Ba deposition does not change the surface structure of the substrate and the YBCO film grows "normally" on the substrate with no intermediate layer formed. Here the word "normally" means that the film grows exclusively in the 45° orientation because this orientation results in a smaller lattice mismatch to the substrate. On the sputtered surface, however, the W implantation, and to some extent the Ar ion sputtering, introduce some kind of structural and chemical changes in the surface layer of the substrate, which lead to Ba diffusion into the MgO surface layer. This diffusion forms on the substrate surface a layer of $Ba_xMg_{1-x}O$ that functions as a buffer for the subsequent film growth. The initial deposition of Ba also helps in the formation of this buffer layer. The presence of the buffer layer on the MgO surface avoids the large lattice mismatch between MgO and 0° oriented YBCO film and makes the 0° oriented growth energetically favorable.

At this moment, it is not clear what structural and chemical changes are induced by the W ion implantation during sputtering. One possible change is that W ions create a large amount of vacancies in MgO on their path of implantation due to their large mass. The existence of these vacancies enhances the diffusion of Ba atoms later in the film growth process. The consistency between the thickness of the diffusion layer and the depth of the W implantation (both of them are a few nm) seems to support this assumption. The reason why Ba has significantly stronger diffusion than Y and Cu may be that Ba has the same valance structure as Mg in contrast to Y and Cu. Another possible effect of the W ion implantation is the change in the electronic structure of the MgO surface layer since W has a different number of valance electrons compared to Mg. The details on these structural and chemical changes and the exact structure and composition of the intermediate layer induced by the ion sputtering are the objects of further investigations.

IV. CONCLUSION

The mechanism of the sputter-induced epitaxy modification (SIEM) occurring in YBCO films grown on MgO (001) surfaces has been investigated through a series of film growth and characterization experiments. The effects of several factors on the occurrence of SIEM are studied. First, the surface morphology change caused by ion sputtering is found not to be a major factor. Although the sputtered surface is rougher on a large scale, no significant difference regarding atomic-scale features on the sputtered and nonsputtered surfaces is observed. Second, the Ar implantation into the substrate is also excluded as a major factor because the Ar concentration on the sputtered surface saturates before any SIEM occurs. Third, W ion implantation is identified as one of the most important factors that induce SIEM. This is confirmed by comparing the film growth results using ion guns with and without W filament. Finally, the initial Ba deposition is found to be essential to control the film growth orientation.

By analyzing the experimental results regarding these relevant factors and by studying the microstructure and elemental distribution of the resultant YBCO/MgO interfaces, the mechanism of SIEM is elucidated as follows. On the nonsputtered MgO (001) surface YBCO grows in the 45° orientation because of the smaller lattice mismatch in this orientation. On the sputtered surface the W implantation associated with the sputtering induces some structural and chemical changes that cause Ba diffusion into the damaged MgO surface layer and form a $Ba_xMg_{1-x}O$ buffer layer on top of the substrate surface. The formation of this buffer layer is also helped by the initial Ba deposition in the POMBE growth. This buffer layer relieves the large lattice mismatch between MgO and the 0° oriented YBCO layer and thus makes the 0° growth possible on the sputtered surfaces.

ACKNOWLEDGMENTS

The authors are grateful to V. Dravid, W. A. Chiou, and Y. Y. Wang for help in the microanalysis, to R. Csencsits, H. Zhang, and W. Sinkoer for their help in the HREM experiments, and to L. J. Thompson and F. R. Ding for help with TRIM and RBS simulation. This work is supported by the National Science Foundation, under Contract No. DMR 91-20000 (YH, BVV) and the United States Department of Energy under Contract No. W-31-109-ENG-38 (KLM).

REFERENCES

1. K. P. Daly, W. D. Dozier, J. F. Burch, S. B. Coons, R. Hu, C. E. Platt, and R. W. Simon, Appl. Phys. Lett. **58**, 543 (1991).
2. C. L. Jia, B. Kabius, K. Urban, K. Herrmann, J. Schubert, W. Zander, and A. I. Braginski, Physica C **196**, 211 (1992).
3. D. Dimos, P. Chaudhari, and J. Mannhart, Phys. Rev. B **41**, 4038 (1990).
4. D. Dimos, P. Chaudhari, J. Mannhart, and F. K. LeGoues, Phys. Rev. Lett. **61**, 219 (1988).
5. H. B. Lu, T. W. Huang, J. J. Wang, J. Lin, S. L. Tu, S. J. Yang, and S. E. Hsu, IEEE Trans. Appl. Supercond. **3**, 2325 (1993).
6. K. Char, M. S. Colclough, S. M. Garrison, N. Newman, and G. Zaharchuk, Appl. Phys. Lett. **59**, 733 (1991).
7. R. P. J. Ijsselsteijn, J. W. M. Hilgenkamp, M. Eisenberg, C. Vittoz, J. Flokstra, and H. Rogalla, J. Allo. Comp. **195**, 231 (1993).
8. N. G. Chew, S. W. Goodyear, R. G. Humphreys, J. S. Satchell, J. A. Edwards, and M. N. Keene, Appl. Phys. Lett. **60**, 1516 (1992).
9. N. G. Chew (1992), private communication.
10. B. V. Vuchic, K. L. Merkle, K. A. Dean, D. B. Buchholz, R. P. H. Chang, and L. D. Marks, J. Appl. Phys. **77**, 2591 (1995).
11. B. V. Vuchic, K. L. Merkle, J. W. Funkhouser, D. B. Buchholz, K. A. Dean, R. P. H. Chang, and L. D. Marks, IEEE Trans. Appl. Supercond. (1995).

12. B. V. Vuchic, K. L. Merkle, P. M. Baldo, K. A. Dean, D. B. Buchholz, R. P. H. Chang, H. Zhang, and L. D. Marks, Physica C **270**, 75 (1996).
13. D. B. Buchholz, J. S. Lei, S. Mahajan, P. R. Markworth, R. P. H. Chang, B. Hinds, T. J. Marks, J. L. Schindler, C. R. Kannewurf, Y. Huang, and K. L. Merkle, Appl. Phys. Lett. **68**, 3037 (1996).
14. M. Aindow, T. T. Cheng, and D. D. Norris, Philos. Mag. Lett. **74**, 267 (1996).
15. A. Gervais and D. Keller, Physica C **246**, 29 (1995).
16. Y. Huang, B. V. Vuchic, D. B. Buccholz, K. L. Merkle, and R. P. H. Chang, Proc. 54th Annu. meeting, MSA, edited by G. W. Bailey (San Francisco Press, San Francisco, CA, 1996), p. 372.
17. D. M. Hwang, T. S. Ravi, R. Ramesh, S-W. Chan, and C. Y. Chen, Appl. Phys. Lett. **57**, 1690 (1990).
18. M. Kamei, Y. Aoki, S. Ogota, T. Usui, and T. Morishita, J. Appl. Phys. **74**, 436 (1993).
19. S-T. Lee, S. Chen, L. S. Hung, and G. Braunstein, Appl. Phys. Lett. **55**, 286 (1989).
20. C. LePaven-Thivet, M. Guilloux-Viry, J. Padiou, A. Perrin, M. Sergent, L. A. deVaulchier, and N. Bontempts, Physica C **244**, 231 (1995).
21. Q. Li, O. Meyer, X. X. Xi, J. Geerk, and G. Linker, Appl. Phys. Lett. **55**, 310 (1989).
22. S. McKernan, M. G. Narton, and C. B. Carter, J. Mater. Res. **7**, 1052 (1992).
23. M. G. Norton, L. A. Tietz, S. R. Summerfelt, and C. B. Carter, Appl. Phys. Lett. **55**, 2348 (1989).
24. M. G. Norton and C. B. Carter, J. Cryst. Growth **110**, 641 (1991).
25. M. G. Norton and C. B. Carter, Scanning Microsc. **6**, 385 (1992).
26. S. J. Pennycook, M. F. Chisholm, D. E. Jesson, R. Feenstra, S. Zhu, X. Y. Zheng, and D. J. Lowndes, Physica C **202**, 1 (1992).
27. R. Ramish, D. Hwang, T. S. Ravi, A. Inam, J. G. Barner, L. Nazar, S. W. Chan, C. Y. Chen, B. Dutta, T. Benkatesan, and X. D. Wu, Appl. Phys. Lett. **56**, 2243 (1990).
28. T. S. Ravi, D. M. Hwang, R. Ramesh, S. W. Chan, L. Nazar, C. Y. Chen, A. Inam, and T. Venkatesan, Phys. Rev. B **42**, 10 141 (1990).
29. N. Savvides and A. Katsaros, Physica C **226**, 23 (1994).
30. D. H. Shin, J. Silcox, S. E. Rssek, D. K. Lathrop, B. Moeckly, and R. A. Buhrman, Appl. Phys. Lett. **57**, 508 (1990).
31. S. K. Streiffer, B. M. Lairson, C. B. Eom, B. M. Clemens, and J. C. Bravman, Phys. Rev. B **43**, 13007 (1991).
32. H. Suzuki, Y. Fujiwara, Y. Hirotsu, T. Yamashita, and T. Oikawa, Jpn. J. Appl. Phys. **32**, 1601 (1993).
33. M. Suzuki and H. Sakurai, IEEE Trans. Appl. Supercond. **5**, 1233 (1995).
34. C. Traeholt, J. G. Wen, V. Svetchnikov, and H. W. Zandbergen, Physica C **230**, 297 (1994).
35. M. Cotter, S. Campbell, R. G. Edgell, and W. C. Mackpodt, Surf. Sci. **197**, 208 (1988).
36. D. B. Buchholz, J. S. Lei, S. Mahajan, P. R. Markworth, R. P. H. Chang, B. Hinds, T. J. Marks, Y. Huang, and K. L. Merkle, J. Allo. Comp. **251**, 278 (1997).
37. Y. Huang, B. V. Vuchic, P. Baldo, K. L. Merkle, D. B. Buchholz, S. Mahajan, J. S. Lei, P. R. Markworth, and R. P. H. Chang, in *Interfacial Engineering for Optimized Properties*, edited by C. L. Briant, C. B. Carter, and E. L. Hall (Mater. Res. Soc. Symp. Proc. **458**, Pittsburgh, PA, 1997), p. 497.
38. S. J. Duray, D. B. Buchholz, S. N. Song, D. S. Richardson, J. B. Ketterson, T. J. Marks, and R. P. H. Chang, Appl. Phys. Lett. **59**, 1503 (1991).
39. Y. Huang and K. L. Merkle, in *Specimen Preparation for Transmission Electron Microscopy of Materials IV*, edited by R. M. Anderson and S. D. Walck (Mater. Res. Soc. Symp. Proc. **480**, Pittsburgh, PA, 1997), p. 235.
40. M. Cotter, S. Campbell, L. L. Cao, R. G. Egdell, and W. C. Mackrodt, Surf. Sci. **208**, 267 (1989).